

Bifurcated Mechanical Behavior of Deformed Periodic Porous Solids

By Srikanth Singamaneni, Katia Bertoldi, Sehoon Chang, Ji-Hyun Jang, Seth L. Young, Edwin L. Thomas,* Mary C. Boyce,* and Vladimir V. Tsukruk*

The transformation of periodic microporous structures fabricated by interference lithography followed by their freezing below glass transition is described. Periodic porous microstructures subjected to internal compressive stresses can undergo sudden structural transformation at a critical strain. The pattern transformation of collapsed pores is caused by the stresses originated during the polymerization of acrylic acid (rubbery component) inside of cylindrical pores and the subsequent solvent evaporation in the organized microporous structure. By confining the polymerization of acrylic acid to localized porous areas complex microscopic periodic structures can be obtained. The control over the mechanical instabilities in periodic porous solids at a sub-micron scale demonstrated here suggests the potential mechanical tunability of photonic, transport, adhesive, and phononic properties of such periodic porous solids.

1. Introduction

Mechanical instabilities are ubiquitous phenomena observed at all length scales in a wide range of materials in both natural and man-made systems.^[1–12] Of various types of instabilities, such as wrinkling, fingering, snap-through, and Rayleigh instabilities, to name a few, buckling is the most commonplace for elastic and elasto-plastic materials. For instance, reduction in the elastic energy due to out-of-plane periodic bending caused by either elastic compression or stretching manifests itself in a wide range of phenomena such as wrinkling of the skin, textured cream on milk, and the edges of leaves. Buckling instabilities in metals, ceramic, and polymeric thin films have received intense attention

in the last few years. The thin-film buckling phenomenon has been exploited as a novel metrology technique for measuring elastic moduli of nanoscale polymeric films, composite nanomembranes, and 1D and 2D nanostructures, for which conventional mechanical testing approaches cannot be readily applied.^[5–7,9,10]

Buckling instabilities have also been demonstrated to be valuable in controlling adhesion, enabling flexible electronics, fabricating microfluidic structures, providing means for micro- and nanopatterning and optical microdevices based upon microgratings.^[13–17] Very complex and highly localized buckling instabilities patterns have been achieved in thin metal and polymer films by various techniques such as patterning metal

nanoparticles in polymer films, local oxidation of the elastomeric substrate. This phenomenon led to a patterned hard skin or patterned adhesion between the film and substrate well controlled by local mechanical stress distribution.^[1,6,18]

Among recent novel structured materials, microscopic analogs of periodic cellular structures in which the periodicity and the pore size are in the sub-micrometer scale are gaining interest as prospective base for a wide variety of applications ranging well beyond structural materials. Current and prospective applications of these structured materials (sometimes called microframes) include 3D photolithography, photonic, and phononic band gap materials, microfluidic networks, porous biomaterials as tissue engineering scaffolds, and DNA–protein microarrays.^[19–25] When subjected to external stresses caused by direct mechanical loading or internal stresses due to changes in osmotic pressure, or differential thermal expansion, or partial swelling, the periodic porous microstructure can become unstable at a certain critical stress. Such mechanical instability might lead to dramatic transformation of the initial periodic structure, a phenomenon rarely addressed and rarely discussed on a quantitative level.

While the buckling in thin films results in highly periodic surface relief patterns, buckling in periodic porous and bi-component materials might result in much more complicated pattern transformation.^[26] Indeed, peculiar and reversible pattern transformation in periodic elastomeric structures subjected to a simple load has been already uncovered^[11,27,28] and intriguing deformational behavior and fracturing of periodic solids has been reported.^[29] Furthermore, the instability in surface relief elastomeric structures has been employed to pattern nanoparticle distribution.^[30] We have recently demonstrated the pattern

[*] Prof. E. L. Thomas, Dr. J.-H. Jang
Department of Materials Science and Engineering and
Institute of Soldier Nanotechnologies
Massachusetts Institute of Technology, Cambridge, MA (USA)
E-mail: elt@mit.edu

Prof. M. C. Boyce, Dr. K. Bertoldi
Department of Mechanical Engineering
Massachusetts Institute of Technology
Cambridge, MA (USA)
E-mail: mcboyce@mit.edu

Prof. V. V. Tsukruk, S. Singamaneni, S. Chang, S. L. Young
School of Materials Science and Engineering and
School of Polymer, Textile, and Fiber Engineering
Georgia Institute of Technology, Atlanta, GA (USA)
E-mail: vladimir@mse.gatech.edu

DOI: 10.1002/adfm.200801675

transformation in porous elasto-plastic solids following the polymerization of rubbery component in the pores which resulted in the pore collapse.^[31] We discovered the intriguing pattern of buckling instabilities initiated by the compressive stresses generated inside the cylindrical pores by rubbery materials grafted to the walls in the course of its polymerization and solvent evaporation.

In this paper, we describe in detail the triggering and mechanistic aspects of such instabilities responsible for pattern transformation in periodic porous elasto-plastic solids. The porous, periodic, solid polymer structures with different symmetries employed here have been fabricated with multiple laser beam interference lithography (IL) from a negative photoresist.^[32] The surface morphology of these transformed materials was studied with atomic force microscopy (AFM) and internal stress distribution in the transformed structures has been addressed by confocal Raman microscopy. Furthermore, we demonstrated the micropatterning of such mechanical instabilities in periodic, porous solids by confining the compressive stresses to predetermined locations. The confinement of the compressive stress in one and two dimension resulted in higher order, complex microscopic periodic porous structures as discussed here in great detail. Numerical simulations with nonlinear finite element analysis (FEA) were employed to better understand the mechanics of the experimentally observed pattern transformation and elucidate the role of general and localized compressive stress distribution and coupled buckling-rotation of microstructural elements. Finally, we demonstrated the precise replication of the topographical features of the transformed pattern in polystyrene using soft lithography approach.

2. Results and Discussion

2.1. Pattern Transformation as a Result of Mechanical Instabilities

The periodic porous polymer structures studied here have been fabricated with IL from a common negative photoresist, epoxy derivative of a bisphenol-A Novolac photocurable resin, SU8, which is widely utilized in photolithography technology well established in our laboratories (see Experimental Section for details).^[33–36]

Figure 1b and c shows AFM images of the pristine microframes with the corresponding 2D fast Fourier transforms (FFTs; insets) reflecting the square lattice symmetry of cylindrical pores. The periodicity of the square lattice was 830 nm, the radius of the cylindrical pores was 190 nm and the porosity was 20%, as determined from AFM and scanning electron microscopy (SEM) studies. The corresponding oblique lattice microframe fabricated in a similar manner had a periodicity of 1 μm , a pore radius of 200 nm, and a porosity of 35%. The thickness of the microframe structures was 3 μm , making the aspect ratio nearly 8. AFM nanomechanical measurements showed the average modulus of the SU8 IL structures to be 1.3 GPa with higher elastic modulus for nodes and continuous gradient of crosslinking density along struts.^[37,38]

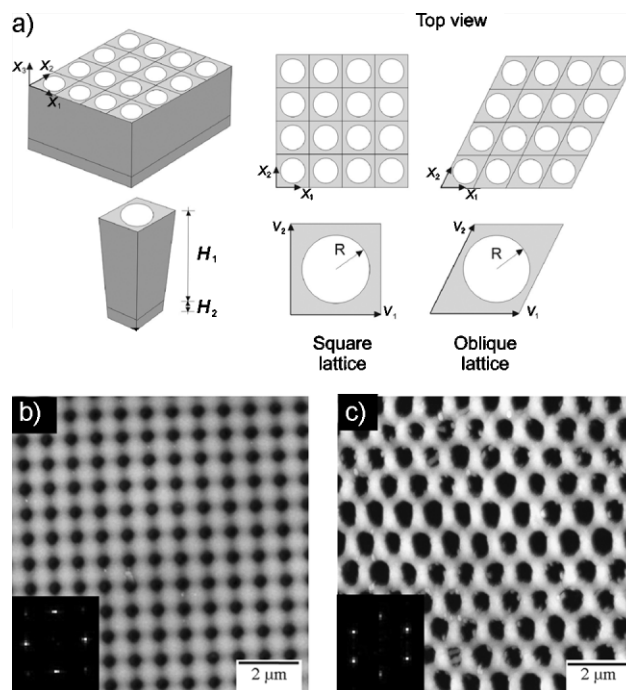


Figure 1. a) 4×4 periodic representative volume elements (top row) and corresponding primitive cells (bottom row) for square and oblique arrays of cylindrical pores. AFM images of the pristine microframe structure with b) square and c) oblique lattices and corresponding FFT patterns (insets).

We verified that conventional filling of the SU8 microframe porous structure with a rubbery phase by employing spin coating and capillary driven infiltration from 2% polybutadiene (PB) solution does not affect the initial porous SU8 structure.^[37] The AFM images shown in Figure 2a and b (topography and phase) clearly demonstrated the finely separated PB microphases localized within the pores forming a characteristic checkerboard pattern. Neither the shape nor the size of the pores exhibited any noticeable changes following the infiltration process.

In a sharp contrast, in situ solution photopolymerization of acrylic acid monomer performed directly in the cylindrical pores resulted in grafting of the polymer to the SU8 walls and eventually in complete reorganization of the initial porous structure. It has been demonstrated that trace amounts of triarylsulfonium hexafluoroantimonate (initiator) which remains within cured SU8 acts as a source of free radicals, initiating UV-mediated grafting of PAA onto the surface of the SU8.^[39] Figure 3 illustrates the surface modification, infiltration of the monomer and subsequent polymerization of the acrylic acid in the pores of the SU8 structure. The slow evaporation of the water from inside of open cylindrical micropores causes the swollen PAA network grafted to the pore walls to shrink significantly, resulting in high compressive stresses. These stresses resulted in a dramatic transformation of the periodic circular holes to ellipses in the case of the square lattice and sheared ellipses in the case of the oblique lattice as is discussed below (Fig. 4).

As a result of this transformation of porous structure, a dramatically different lattice with perfectly regular, non-trivial geometry was observed across the macroscopic surface area (Fig. 5a). The initial square array of cylindrical micropores has

been transformed into periodic, mutually orthogonal, highly collapsed elliptical pores. Transformed regions are extremely uniform extending to surface areas up to few millimeters. On the other hand, the oblique lattice has been transformed into an array of sheared pores with the shear direction alternating back and forth from row to row resembling a common herringbone pattern (Fig. 5b).

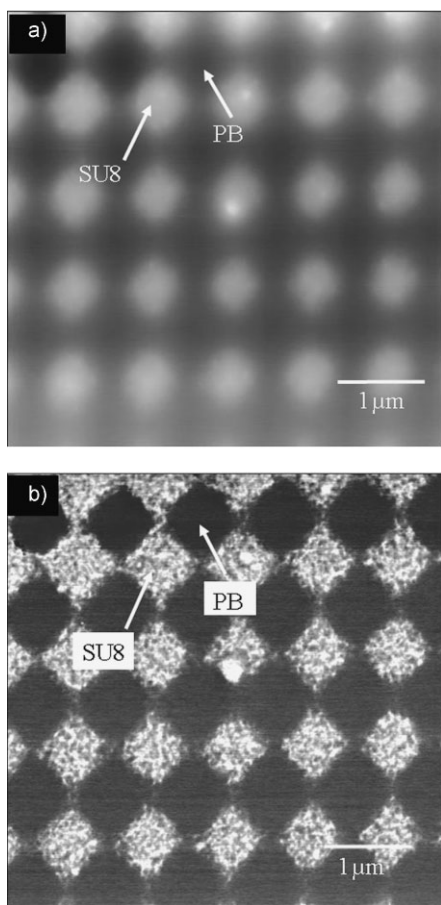


Figure 2. AFM image of square porous SU8 structure filled with PB by capillary infiltration method, a) topography and b) phase, showing the distinct rubber and glassy phases organized in a checkerboard pattern.

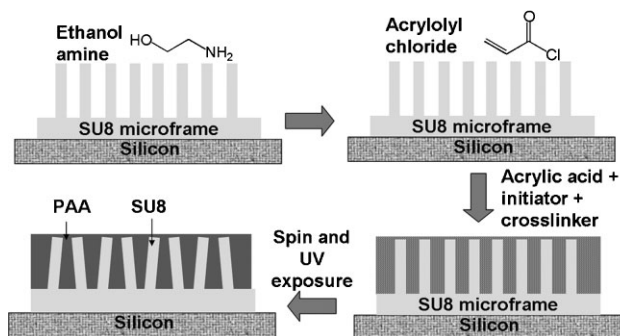


Figure 3. Process steps involved in the in situ polymerization of the acrylic acid in the SU8 structures.

The AFM image depicted in Figure 6 identifies the nodes (elevated round areas) and struts (ridges connecting nodes) of the square lattice microframe structure. At a microscopic level, the pattern transformation can be related to bending of the struts in alternate directions (along x_1 and x_2) and the rotation of the nodes in clockwise and anticlockwise directions^[27] as indicated on the AFM image (Fig. 6). The resulting instabilities are frozen after

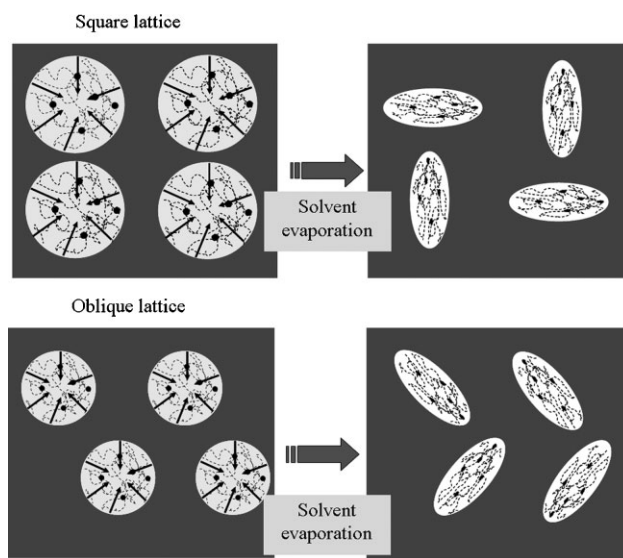


Figure 4. Schematic depicting the transformation in square and oblique lattices.

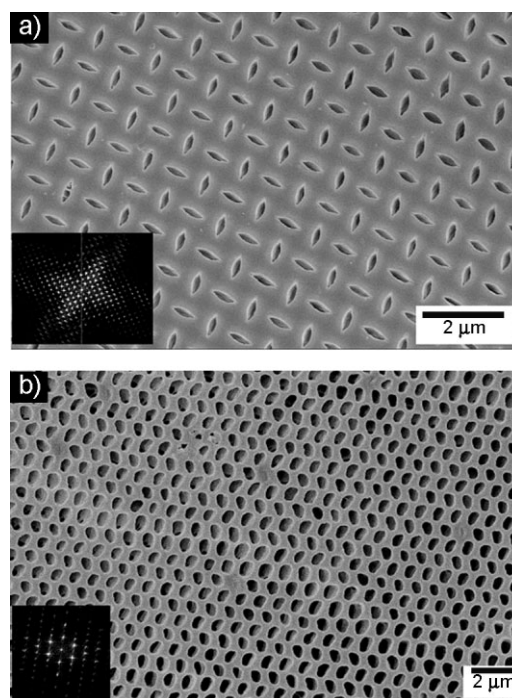


Figure 5. SEM images of transformed patterns of a) square lattice and b) oblique lattice showing the large-scale uniformity of the transformed pattern. Insets show the FFTs of the transformed patterns.

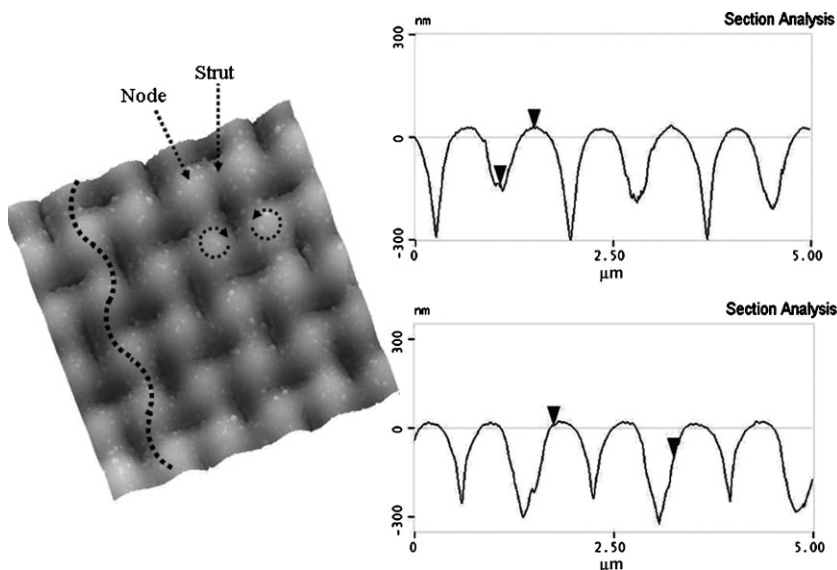


Figure 6. AFM topographical image ($5 \times 5 \mu\text{m}^2$) of the transformed pattern showing the deformation modes of the struts (bending) and the nodes (rotation) on square lattice and the cross-sections along the (01) and (10) directions showing the double bump morphology.

transformation and can be relaxed only after extended annealing at temperature close to glass transition temperature of SU8. The pattern of alternating elliptical micropores is identical along x_1 and x_2 directions with characteristic, double-bump shape reflecting alternating depth of the AFM tip penetration along short and long axes of the collapsed pores caused by its interaction with narrowing, slit-like pores (Fig. 6, see cross-sections in different directions).

2.2. Numerical Analysis of Mechanical Instabilities

For further insight into the mechanics of the pattern transformation observed here, numerical investigations of the behavior of the periodic microporous solids were conducted utilizing nonlinear FEA (see Experimental Section).^[11,27] First, the instabilities of the infinite periodic porous solid are investigated conducting Bloch wave analyses and then load-displacement analyses are conducted to capture the critical transformation event and the post-transformation behavior.^[40]

The bifurcation FEA analysis demonstrates that indeed during the initial deformation, at a critical point the square array of cylindrical pores undergoes an instability transformation. This symmetry change results in a four times enlarged representative cell now consisting of two primitive cells in both lattice directions (Fig. 7a). The displacement field calculated for such a compression confirms the rotation of the nodes and the resulting buckling of the struts as was suggested from AFM imaging (Fig. 6). The oblique array is characterized by a critical instability as well resulting in an enlarged representative cell now consisting of one primitive cell in the horizontal direction and two primitive cells along the other lattice direction (Fig. 7b).

The variation of the eigenmode through the thickness of the specimen for the square array confirms that the transformed pattern gradually develops through the thickness and

corresponds well to the SEM image of the transformed structure (Fig. 8). Such a vertical gradient is caused by the constraint generated by the substrate on the lateral deformation in the vicinity of the buffer layer. Furthermore, the same critical eigenmode is detected at the same macroscopic strain level both when the bottom surface is fixed only in x_3 direction and in all three directions, suggesting only a small influence of the boundary constraint on the behavior of the porous solids at distance larger than one-third of the total thickness. It is worth noting that a gradient transformation along the thickness was suggested earlier (but not confirmed experimentally) as a main cause of pattern transformation of swollen porous elastomers.^[30]

2.3. Internal Stresses Probed by Confocal Raman Microscopy

The dual (elastic–plastic) nature of the SU8 material deformation locks in the mechanical instabilities after the release of the external stress with internal stresses dissipated to a great extent as was confirmed by Raman spectroscopy.^[41] Mapping of peak intensities with confocal Raman microscopy, sensitive to local stresses, confirmed uniform distribution of internal stresses with similar pattern in pristine and the transformed patterns. Figure 9a shows the confocal Raman map of the intensity integrated over 1550 and 1650 cm^{-1} of the pristine and transformed patterns. The Raman peak positions and their relative intensities which are sensitive to active bond vibrations did not exhibit any observable changes between the pristine and transformed solids (compare major bands at 1600 cm^{-1} (backbones, C=C stretching) and at 830 and 1250 cm^{-1} (epoxide ring vibration and ring stretching, respectively; Fig. 9b).^[42,43] Such a similarity suggests a complete relaxation of the stresses for both nodes and struts after the transformation completed and locked. It is worth noting that this observation is in sharp contrast with the instabilities in elastomeric solids, in which the transformed structures exhibit stress concentration in localized areas.^[27]

2.4. Confinement of Mechanical Instabilities

The extent of the pattern transformation across the entire structure can be controlled by localizing the compressive stress in certain areas. Such localized stresses can be achieved by filling predetermined areas of porous structure with acrylic acid monomer solution while preventing the infiltration into the other pores. Capillary transfer lithography (CTL) was employed for selectively depositing a polystyrene pattern with a periodicity of $10 \mu\text{m}$ ($7 \mu\text{m}$ wide polystyrene stripes alternating with $3 \mu\text{m}$ gaps) for selective blocking of certain areas.^[44,45]

Figure 10 illustrates the steps involved in the confined polymerization of the acrylic acid in predetermined, micro-patterned areas. As expected, the photopolymerization in the

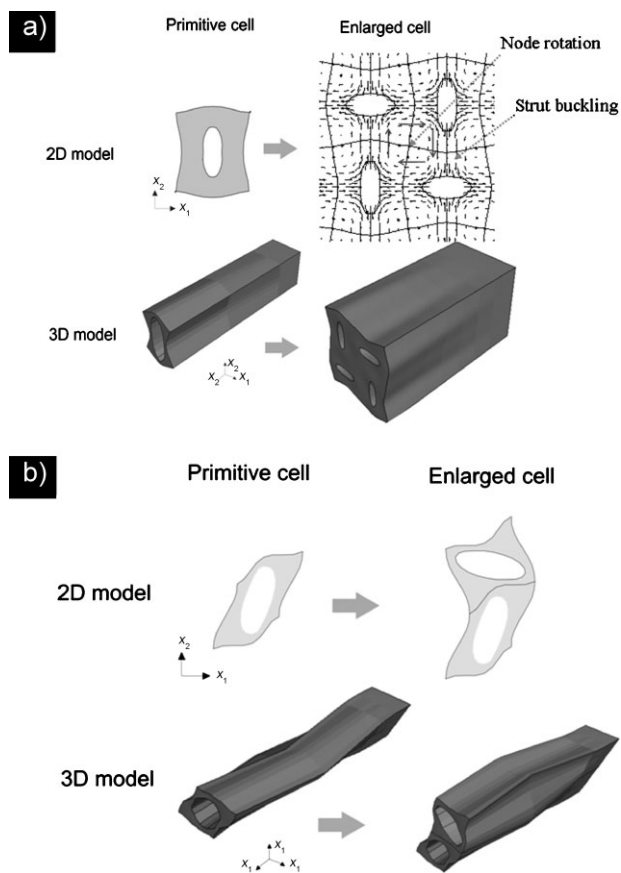


Figure 7. a) Eigenmode of the microscopic instability for the infinite square array of circular holes as predicted by the Bloch wave analysis and the displacement field with arrows showing direction of local displacements (top). The transformed pattern as obtained from the 3D analysis is showed on the bottom. b) Eigenmode of the microscopic instability as predicted by the Bloch wave analysis (top) and transformed pattern as obtained in the 3D analysis (bottom) for the oblique array of circular holes.

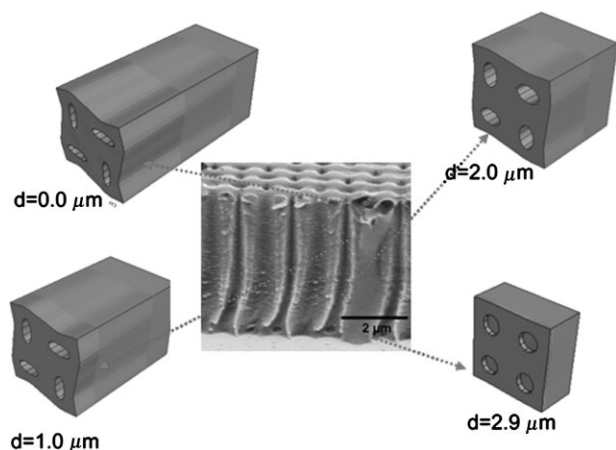


Figure 8. View cuts along the x_1 - x_2 plane at different distances from the top surface and a cross-sectional SEM image of an intentionally fractured microframe depicting the vertical gradient (some shearing is caused by specimen preparation for SEM).

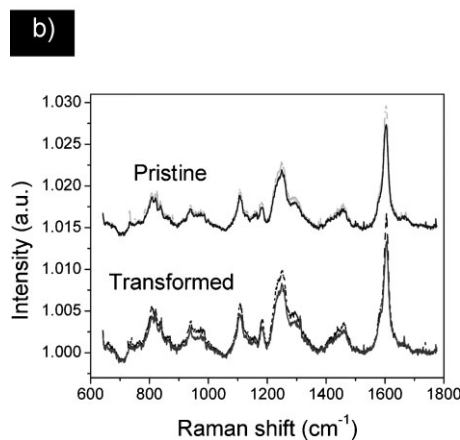
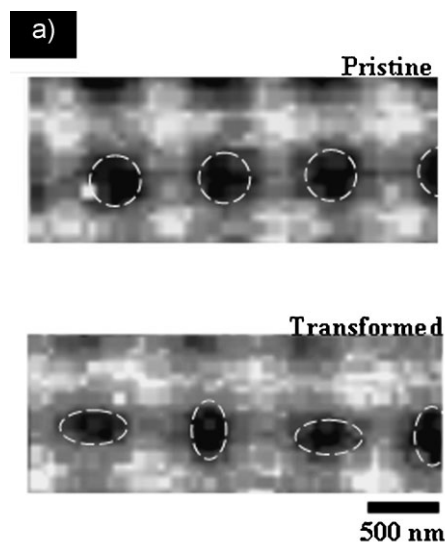


Figure 9. a) Confocal Raman intensity mapping (integrated between 1 580 and 1 620 cm^{-1}) of the pristine and transformed patterns (pixel resolution of about 200 nm limits the visual appearance) and b) average Raman spectra of nodes (solid) and struts (dashed) obtained from the pristine and transformed patterns.

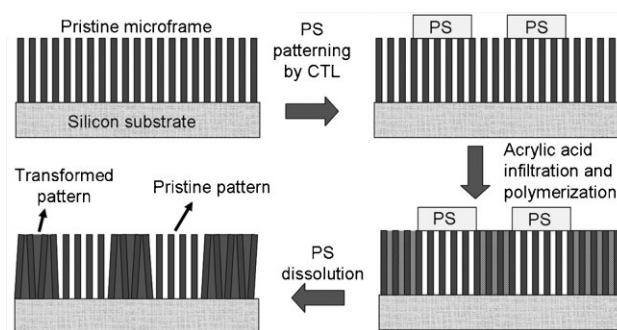


Figure 10. Schematic of experimental routine for patterning the instabilities which involves stamping polystyrene pattern for block acrylic acid infiltration followed by acrylic acid polymerization.

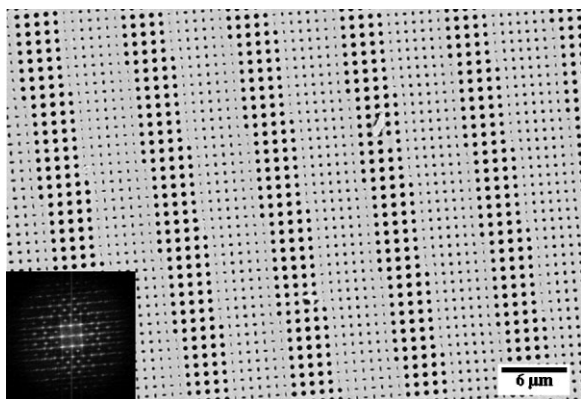


Figure 11. SEM image depicting the large-scale periodic confinement of the mechanical instabilities causing regular transformation pattern (inset shows the FFT of the image).

exposed areas (3- μm wide) resulted in the localized transformed superlattice pattern with periodicity of 10 μm as determined by microstamp spacing (Fig. 11). The SEM image in Figure 11 clearly demonstrates the array of mutually orthogonal elliptical pores (transformed areas) interleaved with the array of circular pores (intact areas) with extremely sharp transition zones between these two regions as discussed below.

Figure 12a shows the higher magnification AFM images of the confined pattern transformation resulting in a hybrid (coexisting pristine and transformed regions) porous structure when the confining polystyrene pattern was parallel to the (10) direction of the microframe square lattice. The AFM image reveals narrow regions with high deformation running at $\sim 45^\circ$ to the lattice direction, releasing the stress caused by overall shrinkage of the volume due to the lateral confinement of transformation to certain localized regions. The cross-section along the line shown in the AFM image depicts the alternating single bump (pristine regions) and double bump morphology (transformed regions; Fig. 12b).

The transition between the pristine and transformed regions in this case is rather sharp, switching from pristine to transformed regions within one unit cell. On the hand, when the polystyrene micropattern was slightly misaligned (by 20°) to the lattice structure [(10) direction], the interface of the pristine and transformed region exhibits a diffused transition with an intermediate topology between the pristine and transformed pattern (Fig. 12c). The stress release in this case occurs by the plane buckling in the form of narrow ridges in between the pristine and transformation regions, as evident from the AFM image (Fig. 12c). The pristine regions are narrow ($\sim 5 \mu\text{m}$) compared to the width of the polystyrene pattern (7 μm), possibly due to

the undercutting of the acrylic acid into the pores at the boundary or from the compressive stresses at the interface.

One important feature common to both of the confined samples was the compression of the transformed regions along the normal direction as compared to the pristine regions as apparent from 3D topography of the micropatterned porous structure and the corresponding cross-section (Fig. 12c and d). In fact, the cross-section analysis reveals that the transformed regions were compressed by $\sim 150 \text{ nm}$ (corresponding to 5% strain) in the vertical direction compared to the pristine porous regions (lower regions in Fig. 12d). The vertical compression is due to the vertical component of the stress exerted during the isotropic collapse of the PAA network during the solvent evaporation. It is worth noting that in recent studies of pattern transformation in elastomers, the authors suggested the vertical compression in the areas of the pattern transformation.^[30] The patterning of instabilities achieved in this study clearly revealed such significant vertical compression in the transformed areas, confirming that the pore collapse occurs not only in the (x,y) plane of the microstructure but also significantly perturbs the porous structure in the z direction.

While the polystyrene parallel stripes pattern confines the mechanical instabilities to one dimension, the more complex pattern comprising of array of polystyrene squares confines the mechanical instabilities in two dimensions (Fig. 13a). The square pattern imposed here has a periodicity of 3 μm with the dimensions of the individual squares being 1.5 $\mu\text{m} \times 1.5 \mu\text{m}$ separated by square areas of the same size. The pattern was

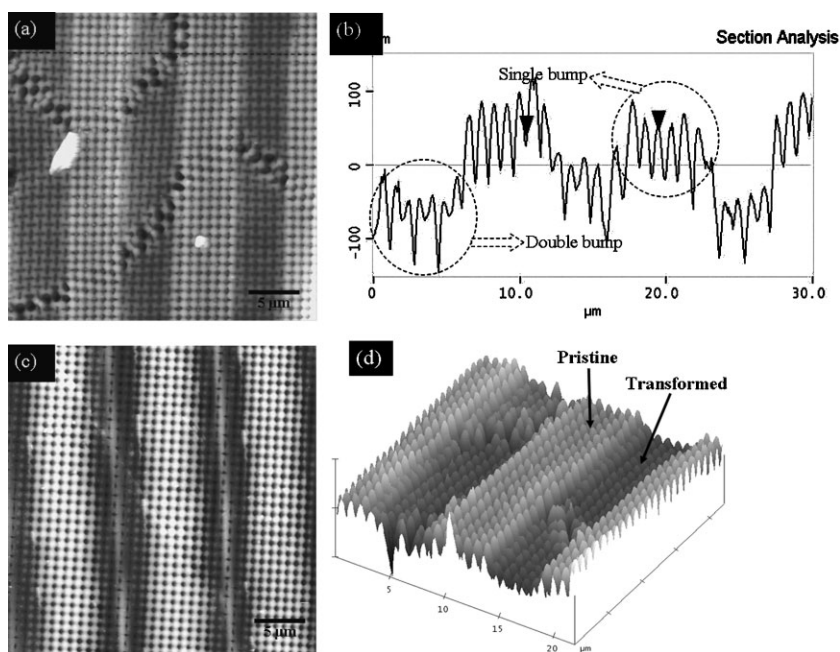


Figure 12. AFM image depicting the periodic transformation with array of circular holes interleaved with array of mutually orthogonal pores. a) Polystyrene pattern aligned with the (10) direction of the microtruss pattern and b) cross-section along the horizontal line (shown on the AFM image) of the interleaved pattern showing the alternating single bump and double bump structure. c) AFM image of the confined pattern transformation when the polystyrene pattern slightly (20°) misaligned with respect to (10) direction. d) 3D AFM image depicting the vertical compression in the transformed areas compared to the pristine areas.

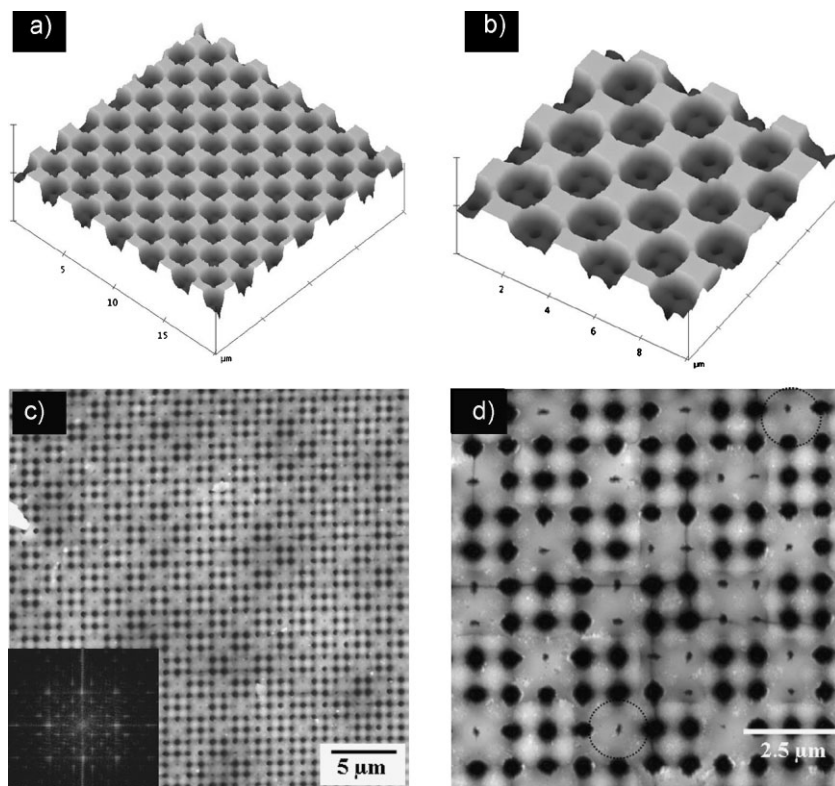


Figure 13. a) AFM image of the uniform square pattern of polystyrene on SU8 structure ($20 \times 20 \mu\text{m}^2$, Z range of $2.2 \mu\text{m}$). b) Higher magnification image clearly depicting the PS pattern and the underneath porous structure and one to three open pores exposed in each open square ($10 \times 10 \mu\text{m}^2$, Z range of $2.0 \mu\text{m}$). Pattern transformation in the microframe owing to the two-dimensional confinement caused by the square patterns of SU8 and polystyrene aligned at 45° with respect to each other (inset shows the FFT depicting overlapped misaligned lattices). c and d) higher magnification of the confined transformation identifying the repeating structure in adjacent cells.

stamped on the porous lattice of the SU8 such that the (10) direction of the polystyrene pattern is at $\sim 45^\circ$ with respect to the (10) direction of the SU8 square lattice. Such a pattern orientation mismatch results in a complex periodic of *superlattice transformed structure* governed by the periodicity of the individual patterns (porous structure itself and polystyrene micropattern) and their relative alignment in (x,y) plane.

Apart from the 2D periodicity, the other significant difference of the square array polystyrene pattern compared to the $10\text{-}\mu\text{m}$ periodic stripe pattern described earlier is the smaller periodicity ($3 \mu\text{m}$). The smaller periodicity results in only one or two open pores followed one or two closed pores in (10) and (01) directions as opposed to nearly five open pores in (10) direction and infinite pores in (01) direction (Fig. 13b). The AFM image of Figure 13c depicts the square array of the transformed pattern and the FFT depicts the overlapping square pattern of the transformed and original lattices oriented 45° with respect to each other. The AFM image in Figure 13d identifies (highlighted by circles) two identical squares in adjacent unit cells. It is apparent that the transformation occurs only partially (in terms of ellipticity of the pores and their orientation), with the pore shape in-between the circular pores and mutually orthogonal ellipses (Fig. 13d).

This partial transformation suggests a finite and very sharp transition region between the pristine and transformed regions which spans over usually two neighboring pores.

Numerical simulations were conducted of both the pattern obtained with polystyrene parallel stripes and square micropatterned arrays to understand the extent of the stresses and corresponding deformation areas. The results of these simulations shown in Figure 14 confirm again that the deformation of porous structures within SU8 material is highly localized and does not extend to more than two or three neighboring cells (Fig. 12a). The width of the transition region is close to the experimentally observed gradient of localized transformation of porous structure (Figs. 12 and 14). The numerical investigations also confirm the experimentally observed intermediate geometry of the deformed pores in the transition regions between the pattern and pristine structures with partially collapsed and intermediately reoriented pores (Fig. 14a).

Indeed, the gradient transformation of porous structures is obvious at the interfacial regions between a pristine and transformed pattern such as that presented in Figure 15 for gradual variation of the degree of pore filling. The transformed pattern extends from a few pores at the top remaining unfilled and so preserving their initial morphology. In this image, one can observe a progressive transformation from a square array of circular holes on the top (initial morphology) to the final transformed pattern of orthogonal collapsed ellipses on the bottom of the region. The gradual alternation of the local orientation of

the ellipsoidal pores confirms the presence of the strong rotational deformation of nodes. Finally, orthogonal orientation is established within few unit cells as highlighted by the arrows in Figure 15.

While only a partial transformation occurs when the polymerization is confined to few pores in (01) and (10) direction, highly localized (confined to just two pores wide) instabilities occur when the polymerization is confined in only one direction. Figure 16 depicts the in situ polymerization conducted in a porous structure with a broad range of topographical features which include squares extending over a few pores and narrow ridges. These topographical features are caused by non-uniform distribution of the acrylic acid monomer in various areas resulting in selective infiltration of the pores in certain areas while the other areas remained pristine. Polymerization and subsequent solvent evaporation resulted in highly confined mechanical instabilities in the localized areas where the infiltration of the monomer occurred.

Figure 16a depicts the AFM image with transformed localized areas interconnected by transformed narrow stripes. Figure 16b shows the narrow transformed pattern (two unit cell wide) along the (11) direction. The transformed pattern exhibits highly

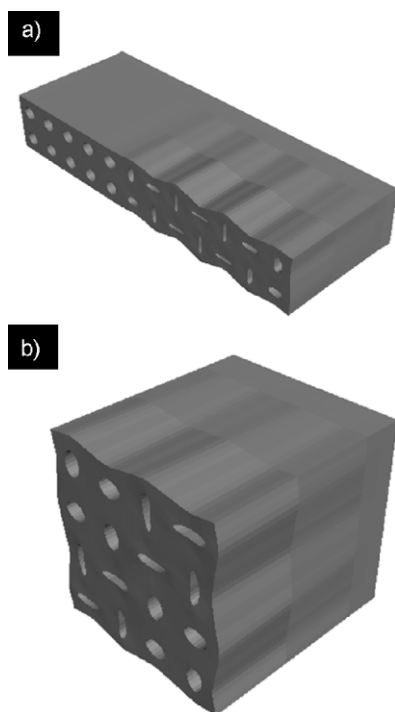


Figure 14. Eigenmode of the microscopic instability for the confined square array of circular holes as predicted by the Bloch wave analysis for a) one-dimensional stripe confinement (2×6 cells) and b) two-dimensional squared confinement (2×2 cells).

deformed concave pores owing to the high degree of localization of the pattern transformation. Furthermore, the pores adjacent to the transformed areas on either sides exhibit large deformation to accommodate the bending of the struts in the transformed regions. The transformation observed here suggests that a complete and highly localized transformation can be achieved when the compressive stresses are confined to one dimension as opposed to the partial transformation in the case of the confinement in two dimensions. The high degree of bending of the struts to accommodate narrow transformed regions shows the excellent mechanical properties and elasto-plastic nature of the SU8 struts.

2.5. Replication of Transformed Pattern

To extend the range of application of pattern transformation harnessed by mechanical instabilities in periodic porous structures, it is highly desirable to extend the range of materials where such transformed periodic structures can be achieved or stored. As a first step towards this goal, we conducted additional studies and confirmed that the topographical features of the transformed pattern can be replicated in a common glassy polymer, polystyrene, by using CTL process as depicted in Figure 17a.^[44]

The process involves in the fabrication of a negative replica (stamp) of the transformed pattern from SU8 structures by using

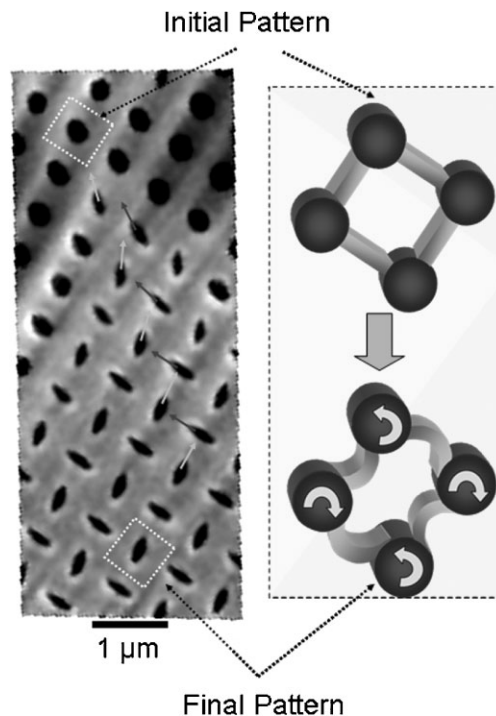


Figure 15. SEM image of the square lattice showing the gradual transformation from a pristine square unit cell of cylindrical pores to the final transformed pattern, and schematic representation of the transformation highlighting the deformation of the individual elements of the microframe structure.

PDMS. The stamp is then used to replicate the transformed pattern in polystyrene (Fig. 17a). The AFM image in Figure 17b shows the resulting polystyrene replica with mutually orthogonal ellipses resembling those in the transformed master, although the level of collapse is less dramatic than in the original microstructure. Based upon this preliminary data, we suggest that this replication technique can be extended to generate more complex polymeric patterns using various patterned instabilities as masters. Furthermore, the stamped patterns can be employed as physical masks for patterning various nanostructured materials for tuning the optical properties of the assembled superlattices.

3. Conclusions

In conclusion, we have demonstrated the onset of buckling instabilities in porous elasto-plastic solids upon polymerization of additional rubbery component inside cylindrical pores which lead to a dramatic pattern transformation. Owing to the elasto-plastic nature of the porous structure, the transformed pattern is frozen and stable as opposed to the elastomeric counterparts, which return to the pristine structure once the external pattern is removed.

We suggest that localized polymerization of acrylic acid within cylindrical pores resulted in confined mechanical instabilities leading to a complex hierarchical porous structure comprised of regularly collapsed pores with alternating orientation. Moreover,

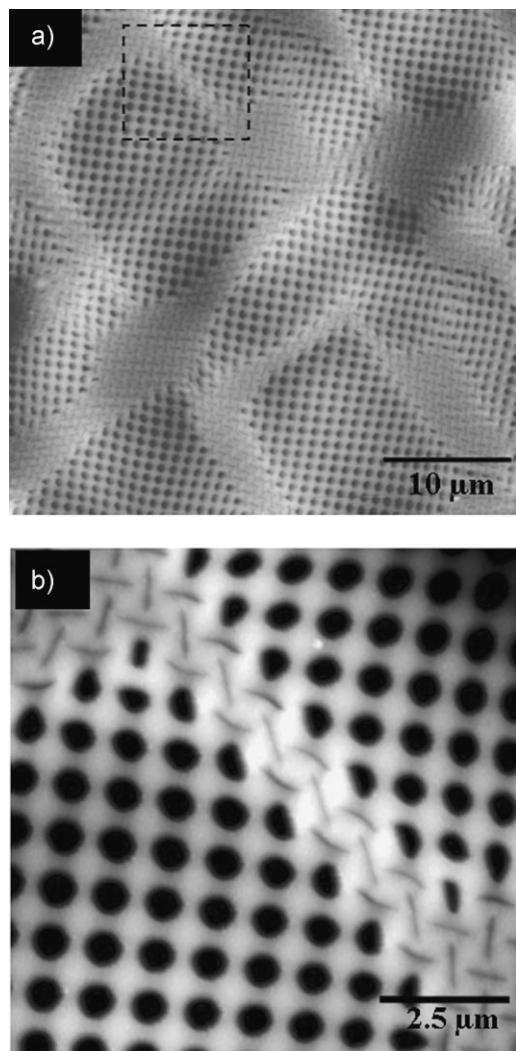


Figure 16. AFM images of mechanical instabilities in a microframe with a variety of topographical features resulting localized transformation of the pattern. a) AFM image depicting the transformed pattern localized to certain areas, connected by narrow ridges. b) Higher magnification image of a single ridge showing the large curvature the struts undergo when the transformed pattern is localized to two adjacent unit cells.

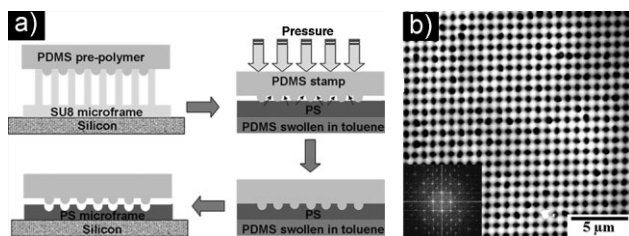


Figure 17. a) Schematic illustrating the CTL replication of the transformed pattern and b) AFM topographical image of replicated polystyrene structure with mutually orthogonal ellipses (inset shows the corresponding FFT).

we have observed a controlled transformation when the polymerization can be confined in two dimensions to highly localized areas which include only two to three neighboring pores. On the other hand, complete transformation with highly collapsed pores can be achieved when the transformation is confined in only one dimension. Finally, we have also demonstrated the replication of the topographical features of the transformed pattern in other polymers using the CTL process.

We believe that the mechanism of transformation of organized microporous solids via localized bifurcation of the primitive cell with rotation of nodes combined with the bending or buckling of struts can be important in the range of complex physical phenomena critical for diverse fields such as tunable photonic crystals, porous scaffolds for tissue engineering, structures with tunable transport properties, or porous-shape memory alloys in metallic and polymeric stents.

4. Experimental

Fabrication of SU8 Microframes: 2D square and hexagonal patterns were fabricated using multi-beam IL according to the usual procedure [37]. The fabrication involved a two-step sequential, double exposure with a 90° rotation of the sample to the interference pattern of two equal intensity laser beams for the square lattice and single exposure to the interference pattern of three equal intensity laser beams for hexagonal lattice. The transfer of the light intensity pattern into an SU8 photoresist platform via laser-initiated cationic polymerization results in each 2D patterned structure. The Gaussian output from the laser was cleaned up and expanded using a spatial filter and recollimation setup.

The materials platform consisted of Epon-SU8 (Miller Stephensen) as a photoresist (a multi-functional epoxy derivative of a bisphenol-A Novolac), H-Nu 470 (Spectra group) as a photosensitizer which absorbs the visible light and electron transfers to an onium salt, octoxyphenylphenyliodonium hexafluoroantimonate (OPPI; UCB Radcure) as a photoacid generator, and triethylamine to compensate for the non-zero background arising from the interference intensity. The glass substrate was treated with a thin (700 nm) buffer layer of pre-crosslinked SU8 material to assure attachment of the structured polymer film to the substrate via chemical grafting. A 3 μm thick SU8 film was subsequently spin-coated on top of the existing crosslinked SU8 film at a spin speed of 2000 rpm. The IL exposure was done using a 532 nm continuous wave Nd:YAG laser with an intensity of 1.5 W for 8–15 s to give the total exposure dose of 12–22 J cm⁻². After baking the 3-μm-thick film at 75 °C for 3 min, the resultant cationic photopolymerization only takes place in regions that were exposed to high intensities of light. The uncured regions are developed away in propyleneglycol monomethylether acetate (PGMEA) followed by rinsing with isopropanol. No further heat treatment was applied. The glass transition temperature of the SU8 cured under similar conditions (including the 5 min UV exposure during the acrylic acid) was found to be 120 °C from the DMA measurements.

In Situ Polymerization of Acrylic Acid in Sub-Micron Pores: To fabricate filled microstructures (Fig. 3), pristine microframes were treated with ethanol amine to reduce the hydrophobicity and induce surface hydroxyl groups [46]. Following the ethanol amine treatment (which resulted in a decrease in the contact angle from 90 to 30°), the sample was thoroughly washed in Nanopure water and placed in a vial containing 1% acryloyl chloride in ethyl ether for 90 min. AFM imaging at this stage in various locations of the sample revealed no signs of transformed pattern. Then, the sample was washed thoroughly and immersed in a 20% acrylic acid solution with 5% UV initiator and 2% UV crosslinker (acryl amide), allowing acrylic acid solution to infiltrate pores. Finally, the sample was exposed to UV light (365 nm, 20 mW cm⁻²) to initiate polymerization of AA. The pH of the monomer with initiator and crosslinker was 2.3 keeping the carboxylic moieties on the PAA are in neutral state. The crosslinked PAA materials filling the micropores is in a swollen state in water (73%).

Patterning Instabilities: To localize and pattern the instabilities, patterns of polystyrene were employed as physical mask on the microframe to prevent acrylic acid infiltration into the desired pores. The samples were treated with ethanol amine to reduce of the hydrophobicity and stamped with a pattern of polystyrene (with 10- μm periodicity) using CTL illustrated in Figure 10 [44,45]. In brief, a PDMS stamp (with 10- μm periodicity) was soaked in toluene for 1–2 min and brought into conformal contact with the polystyrene film on the PDMS substrate (swollen in toluene) and pressed for 1 min. The polystyrene infiltrated the receding portions of the PDMS stamp by capillary action. The pattern was then transferred onto the microframe surface by contact of the PDMS stamp for 1 min.

Numerical Simulations: FEA calculations were conducted within the nonlinear code ABAQUS/Standard, version 6.6-1. In the numerical analyses an infinite array of circular holes has been considered in the x_1 – x_2 plane parallel to the holes, so that the analyses could be conducted both on the primitive cell and on multi-cell representative volume elements (RVEs). To respect the periodicity of the structure a series of constraint equations were applied to the surfaces of the primitive cell (not on the top and bottom surface) providing general periodic boundary conditions [47]. The square array is composed of cylindrical pores with a radius $R = 190$ nm and a primitive cell Y defined by the lattice vectors $\nu_1 = [830\ 0]$ nm and $\nu_2 = [0\ 830]$ nm. The oblique array with a radius $R = 200$ nm is spanned by $\nu_1 = [1000\ 0]$ nm and $\nu_2 = [500\ 1000]$ nm. The stress–strain behavior of the material (photocrosslinked epoxy SU8) is captured using a rate independent elasto-plastic model, since the small rate dependency recently observed does not influence the pattern transformation [48,49]. The initial Young's modulus has been measured to be 1300 MPa and the Poisson's ratio is taken to be 0.33. The other material parameters are derived from values recently measured, taking them to linearly scale with the initial Young modulus. A Mises yield surface and isotropic hardening are used with a yield stress of 60 MPa and a strain hardening modulus of 300 MPa [49].

2D models under plane strain conditions were used to investigate instability performing Bloch wave analyses [11,47]. The mesh was constructed of 6-node, quadratic, 2D elements (ABAQUS element type CPE6H) and a pressure was applied to the void to mimic shrinkage occurring after evaporation of the water. 3D models using 15-node, quadratic, hybrid elements (ABAQUS element type C3D15H) were then constructed and the mesh was perturbed using the critical eigenmode obtained from the Bloch wave analysis. In the 3D models, the pores are considered to be 3- μm long in the x_3 direction and the porous structures are bonded to a substrate that is 700-nm thick. In correspondence with the periodicity of the transformed patterns, RVEs consisting of 2×2 and 1×2 primitive cells are considered to simulate the stress–strain response of the square and oblique arrays, respectively.

Microscopy: The morphology of the pristine and patterned microframes was studied with a Dimension 3000 Atomic Force Microscope (AFM) according to the procedure adapted in our laboratory [50,51]. Field-emission scanning electron microscopy (FESEM, LEO 1530) was used to investigate the pattern transformation in the microframe structures. Raman measurements were performed on both pristine and transformed SU8 structures using Alpha 300R Witek Confocal Raman microscope. Raman measurements were conducted using an Argon laser at 514.5 nm with the incident power below 4 mW. The average spectrum from struts and nodes were obtained by averaging over 40 individual spectra from different locations.

Acknowledgements

The work presented here is supported by NSF-CMS-0709586 grant, the Air Office of Scientific Research, and Institute for Soldier Nanotechnologies of the U.S. Army Research Office (under Contract DAAD-19-02-0002).

Received: November 13, 2008
Published online: February 23, 2009

- [1] N. Bowden, S. Brittain, A. G. Evans, J. W. Hutchinson, G. M. Whitesides, *Nature* **1998**, 393, 146.
- [2] K. Efimenko, M. Rackaitis, E. Manias, A. Vaziri, L. Mahadevan, J. Genzer, *Nat. Mater.* **2005**, 4, 293.
- [3] L. Mahadevan, S. Rica, *Science* **2005**, 307, 1740.
- [4] J. Hiller, J. D. Mendelsohn, M. F. Rubner, *Nat. Mater.* **2002**, 1, 59.
- [5] C. M. Stafford, C. Harrison, K. L. Beers, A. Karim, E. J. Amis, M. R. Vanlandingham, H.-C. Kim, W. Volksen, R. D. Miller, E. E. Simonyi, *Nat. Mater.* **2004**, 3, 545.
- [6] C. Jiang, S. Singamaneni, E. Merrick, V. V. Tsukruk, *Nano Lett.* **2006**, 6, 2254.
- [7] Y. Sun, W. M. Chi, H. Jiang, Y. Y. Huang, J. A. Rogers, *Nat. Nanotechnol.* **2006**, 1, 201.
- [8] R. Gunawidjaja, H. Ko, C. Jiang, V. V. Tsukruk, *Chem. Mater.* **2007**, 19, 2007.
- [9] D.-Y. Khang, J. Xiao, C. Kocabas, S. MacLaren, T. Banks, H. Jiang, Y. Y. Huang, J. A. Rogers, *Nano Lett.* **2008**, 8, 124.
- [10] J. Huang, M. Juskiewicz, W. H. de Jeu, E. Cerda, T. Emrick, N. Menon, T. P. Russell, *Science* **2007**, 317, 650.
- [11] K. Bertoldi, M. C. Boyce, S. Deschanel, S. M. Prange, T. Mullin, *J. Mech. Phys. Solid.* **2008**, 56, 2642.
- [12] J.-T. Chen, M. Zhang, T. P. Russell, *Nano Lett.* **2007**, 7, 183.
- [13] E. P. Chan, E. J. Smith, R. C. Hayward, A. J. Crosby, *Adv. Mater.* **2008**, 20, 711.
- [14] P. Lin, S. Vajpayee, A. Jagota, C.-H. Hui, S. Yang, *Soft Matter* **2008**, 4, 1830.
- [15] Y. Sun, J. A. Rogers, *J. Mater. Chem.* **2007**, 17, 832.
- [16] Y. Sun, W. M. Choi, H. Jiang, Y. Y. Huang, J. A. Rogers, *Nat. Nanotechnol.* **2006**, 1, 201.
- [17] P. J. Yoo, K. Y. Suh, S. Y. Park, H. H. Lee, *Adv. Mater.* **2002**, 14, 1383.
- [18] M.-W. Moon, S. H. Lee, J.-Y. Sun, K. H. Oh, A. Vaziri, J. W. Hutchinson, *Proc. Natl. Acad. Sci.* **2007**, 104, 1130.
- [19] M. Campbell, D. N. Sharp, M. T. Harrison, R. G. Denning, A. J. Turberfield, *Nature* **2000**, 404, 53.
- [20] S. John, *Phys. Rev. Lett.* **1987**, 58, 2486.
- [21] M. Ulbricht, *Polymer* **2006**, 47, 2217.
- [22] M. Théry, V. Racine, A. Pépin, M. Piel, Y. Chen, J.-B. Sibarita, M. Bornens, *Nat. Cell Biol.* **2005**, 7, 947.
- [23] J.-H. Jang, C. K. Ullal, T. Gorishnyy, V. V. Tsukruk, E. L. Thomas, *Nano Lett.* **2006**, 6, 740.
- [24] S. Hollister, *Nat. Mater.* **2005**, 4, 518.
- [25] X. Zhu, Y. Zhang, D. Chandra, S.-C. Cheng, J. M. Kikkawa, S. Yang, *Appl. Phys. Lett.* **2008**, 93, 161911.
- [26] J. Genzer, J. Groenewold, *Soft Matter* **2006**, 2, 310.
- [27] T. Mullin, S. Deschanel, K. Bertoldi, M. Boyce, *Phys. Rev. Lett.* **2007**, 99, 084301.
- [28] K. Bertoldi, M. C. Boyce, *Phys. Rev. B* **2008**, 77, 052105.
- [29] S. Singamaneni, S. Chang, J.-H. Jang, W. Davis, E. L. Thomas, V. V. Tsukruk, *Phys. Chem. Chem. Phys.* **2008**, 10, 4093.
- [30] Y. Zhang, E. A. Matsumoto, A. Peter, P.-C. Lin, R. D. Kamien, S. Yang, *Nano Lett.* **2008**, 8, 1192.
- [31] S. Singamaneni, K. Bertoldi, S. Chang, J.-H. Jang, E. L. Thomas, M. Boyce, V. V. Tsukruk, *ACS Appl. Mater. Interfaces* **2009**, 1, 42.
- [32] J. H. Moon, S. Yang, *J. Macromol. Sci., Part C: Polym. Rev.* **2005**, 45, 351.
- [33] C. K. Ullal, M. Maldovan, E. L. Thomas, G. Chen, Y.-J. Han, S. Yang, *Appl. Phys. Lett.* **2004**, 84, 5434.
- [34] J.-H. Jang, C. K. Ullal, M. Maldovan, T. Gorishnyy, S. Kooi, C. Koh, E. L. Thomas, *Adv. Funct. Mater.* **2007**, 17, 3027.
- [35] J. H. Moon, J. Ford, S. Yang, *Polym. Adv. Technol.* **2006**, 17, 83.
- [36] M. Maldovan, C. K. Ullal, W. C. Carter, E. L. Thomas, *Nat. Mater.* **2003**, 2, 664.
- [37] T. Choi, J.-H. Jang, C. K. Ullal, M. C. Lemieux, V. V. Tsukruk, E. L. Thomas, *Adv. Funct. Mater.* **2006**, 16, 1324.

- [38] J.-H. Jang, C. K. Ullal, T. Choi, M. C. Lemieux, V. V. Tsukruk, E. L. Thomas, *Adv. Mater.* **2006**, *18*, 2123.
- [39] Y. Wang, M. Bachman, C. E. Sims, G. P. Li, N. L. Allbritton, *Langmuir* **2006**, *22*, 2719.
- [40] N. Triantafyllidis, M. D. Nestorovic, M. W. Schraad, *J. Appl. Mech.* **2006**, *73*, 505.
- [41] C. Jiang, H. Ko, V. V. Tsukruk, *Adv. Mater.* **2005**, *17*, 2127.
- [42] G. Socrates, *Infrared and Raman Characteristic Group Frequencies Tables and Charts*, 3rd Ed., Wiley, NY **2001**.
- [43] Y.-T. Chen, D. Lee, *J. Micromech. Microeng.* **2007**, *17*, 1978.
- [44] K. Y. Suh, Y. S. Kim, H. H. Lee, *Adv. Mater.* **2001**, *13*, 1386.
- [45] H. Ko, C. Jiang, V. V. Tsukruk, *Chem. Mater.* **2005**, *17*, 5489.
- [46] M. Nordström, R. Marie, M. Calleja, A. Boisen, *J. Micromech. Microeng.* **2004**, *14*, 1614.
- [47] M. Danielsson, D. M. Parks, M. C. Boyce, *J. Mech. Phys. Solids* **2002**, *50*, 351.
- [48] C.-Y. Wen, W. S. Kim, E. L. Thomas, unpublished.
- [49] L. Wang, M. C. Boyce, C.-Y. Wen, E. L. Thomas, unpublished.
- [50] V. V. Tsukruk, *Rubber Chem. Technol.* **1997**, *70*, 430.
- [51] V. V. Tsukruk, D. H. Reneker, *Polymer* **1995**, *36*, 1791.